

Investigations of CrN/TiO₂ coatings obtained in a hybrid PVD/ALD method on Al–Si–Cu alloy substrate

Marcin STASZUK *

Silesian University of Technology, Faculty of Mechanical Engineering, Konarskiego 18a St., 44-100 Gliwice, Poland

Abstract. The paper addresses an important scientific topic from the utilitarian point of view concerning the surface treatment of Al–Si–Cu aluminum alloys with PVD/ALD hybrid coating deposition. The influence of the conditions of titanium oxide deposition in CrN/TiO₂ coatings on their structure and properties, in particular corrosion resistance, were investigated. The TiO₂ layer was produced by means of the atomic layer deposition (ALD) method with a variable number of cycles. Structural investigations were performed using scanning and transmission electron microscopy (SEM and TEM), atomic force microscopy (AFM), and Raman spectroscopy methods. Electrochemical properties were analyzed using potentiodynamic and electrochemical impedance spectroscopy (EIS) methods. The CrN/TiO₂ hybrid coating with titanium oxide deposited at 500 ALD cycles showed the best corrosion properties. It was also found that the prerequisite for obtaining the best electrochemical properties was the amorphous structure of titanium oxide in the hybrid coatings tested. The high tribological properties of the tested coatings were also confirmed.

Key words: ALD; PVD; hybrid coatings; TiO₂; aluminum alloys; corrosion resistant.

1. INTRODUCTION

Among the most commonly used construction materials today, aluminum alloys are second only to steel. Aluminum products in the form of raw materials, semi-finished and finished products are most often used in the automotive, aerospace and food industries, as well as in the construction, electronics and chemical industries. Aluminum is characterized by its high ductility and density of iron (2.7 mg/m³). Despite its high chemical activity, the material retains relatively high corrosion resistance under normal atmospheric conditions. Aluminum is resistant to water, H₂S, H₂CO₃, and many organic acids and nitrogenous compounds. In contrast, it has no corrosion resistance when exposed to anaerobic acids (HCl, HF), hydroxides (e.g. KOH, NaOH), seawater, and mercury ions [1–5]. Improving the service properties of light metal alloy components is achieved by surface treatment through modification of the surface layer or deposition of protective and anti-wear coatings [5–8].

Chromium nitride CrN is a coating material that is deposited by means of physical vapor deposition (PVD) to achieve both improved wear resistance and improved corrosion resistance. However, in aggressive environments such corrosion protection might not be sufficient. As a result of the natural microstructural defects of this coating, such as, among others, micro craters, the aggressive environment may come into contact with the substrate, and corrosion initiation and development

may occur as a result [9–12]. A solution to this problem can be found in the literature and takes the form of additional deposition of ALD coating on PVD coating, i.e. the formation of a PVD/ALD hybrid coating. Works [13–15] prove the effectiveness of sealing the CrN PVD coating with ALD layers, usually TiO₂ or an Al₂O₃/TiO₂ bilayer. In the publications presented here, the substrate coated in each case was stainless steel or tool steel. In the available literature, there are few studies on hybrid PVD/ALD coatings on light-metal alloy substrates. In [16], the authors Staszuk *et al.* presented the results of a hybrid TiO₂/nanoTiO₂ bimodal coating on an Al–Si–Cu substrate, which exhibits high electrochemical properties but poor mechanical (tribological) properties. Furthermore, in the available publications on CrN/TiO₂ coatings on steel substrates, there is no information on the influence of ALD coating deposition conditions on the resulting titanium oxide microstructure and properties of the resulting PVD/ALD hybrid coating. This study aims to investigate the influence of ALD titanium oxide deposition conditions on the structure and properties of CrN/TiO₂ coatings obtained by the hybrid PVD/ALD method on Al–Si–Cu aluminum alloy substrates.

2. MATERIALS

The substrate to be coated was an aluminum alloy of the Al–Si–Cu type with the chemical composition shown in Table 1. The substrate was heat treated using the precipitation hardening method. Circular specimens with a diameter of 14 mm and thickness of about 5 mm were ground on sandpaper of decreasing gradation. The final step of the substrate was polished

*e-mail: marcin.staszuk@polsl.pl

Manuscript submitted 2022-09-14, revised 2022-11-06, initially accepted for publication 2022-12-30, published in April 2023.

using a diamond slurry with a gradation of 1 μm . After each machining step, the substrates were rinsed with an ultrasonic cleaner, successively in acetone and isopropanol, and dried with a stream of hot air.

Table 1

Chemical composition (%wt.) of the Al–Si–Cu alloy – GDOES

Si	Cu	Fe	Mn	Mg	Zn	Al	Others
9.31	1.62	0.32	0.12	0.51	0.08	87.5	0.54

The substrates prepared in this way were coated with the CrN, TiO₂, and CrN/TiO₂ coatings tested. Chromium nitride coating was performed using an optimized PVD process by magnetron sputtering. The PVD deposition temperature was 200°C.

Titanium oxide coatings were obtained by means of ALD atomic layer deposition using a Picosun ALD R-200 reactor with thermal excitation. Titanium tetrachloride TiCl₄ was the titanium source and distilled water was the oxygen source. The carrier gas was nitrogen. The dosing times and pulsing times of the TiCl₄ precursor and the H₂O reactant were both 0.1 s. Purges times were 4 s and 5 s after TiCl₄ and H₂O, respectively. Three titanium oxide variants were made for a variable number of ALD cycles, i.e. 200, 500, and 1 000 cycles. The deposition temperature was fixed at 200°C.

Hybrid CrN/TiO₂ coatings were obtained by sequentially depositing chromium nitride by PVD and then the same samples were coated with titanium oxide by ALD. For the hybrid coatings, three variants were also performed, depending on the number of ALD cycles. A summary of the coating determinations is shown in Table 2.

Table 2

Research material

Sample designation	PVD coating	ALD coating (number of cycles)	Type of material
Al–Si–Cu uncoated	–	–	reference material
CrN	CrN	–	
TiO ₂ (200)	–	TiO ₂ (200)	
TiO ₂ (500)	–	TiO ₂ (500)	
TiO ₂ (1000)	–	TiO ₂ (1000)	
CrN/TiO ₂ (200)	CrN	TiO ₂ (200)	research material
CrN/TiO ₂ (500)		TiO ₂ (500)	
CrN/TiO ₂ (1000)		TiO ₂ (1000)	

3. METHODOLOGY

Analysis of the chemical composition of the tested substrate was performed using GDOES glow discharge optical emission spectroscopy with the use of the LECO GDS-850 device.

Using scanning electron microscopy SEM and EDS spectroscopy, microstructural studies of the coatings, observations of corrosion products, and damage mechanisms after mechanical property tests were performed.

The study of coating morphology was performed using a Park Systems XE-100 AFM atomic force microscope in non-contact mode. The study area was 1 $\mu\text{m} \times 1 \mu\text{m}$.

Spectroscopic ellipsometry measurements were made using a Sentech SE850E spectroscopic ellipsometer, working in the spectral range of 240–2500 nm, under the Spectra Ray 3 software. Measurements were made in variable angle mode, under a 50–70° angle range. The thickness was determined using a Tauc–Lorentz oscillator.

Investigations of the structure of lamellas from the cross-section of the investigated coatings were carried out using the FEI S/TEM Titan 80–300 transmission electron microscope, operating at a voltage of 300 kV. Observation techniques used were the following: bright field (BF) and high-angle annular dark field (HAADF). For the analysis of the chemical composition, the EDS spectrometer and the energy filter, the Gatan imaging filter (Gatan Tridium 863), were used. Specimens were prepared with the Focused Ion Beam (FIB) technique.

Structure of the investigated coatings was investigated using a Raman spectrometer, which was equipped with an argon-ion laser with a wavelength of 514.5 nm.

The wetting angle θ of the surfaces of the test samples was examined using the sitting drop method. Distilled water and diiodomethane were used as the polar and non-polar liquids, respectively. The surface-free energy (SFE) (γ^s) and the polar (γ_p^s) and dispersion (γ_d^s) components were determined using the Owens–Wendt method. A Surtens Universal system was used for the study, which includes a goniometer, a camera that records droplets of the measuring liquid, and a computer with Surtens 4.5 software.

Electrochemical properties were studied using the potentiodynamic method and EIS electrochemical impedance spectroscopy in a 3.5% NaCl solution using ATLAS 0531EU potentiostat/galvanostat from Atlas Sollich. Corrosion tests were performed in a three-electrode system: the reference electrode was an Ag/AgCl electrode, and the auxiliary electrode was made in the form of a stainless steel wire. The tests were performed at room temperature. Characteristic electrical quantities describing corrosion resistance, i.e. current density (j_{corr}), corrosion potential (E_{corr}) and polarization resistance (R_{pol}), were determined using the Tafel method. The results of the EIS analysis are presented in the form of Nyquist and Bode diagrams. An equivalent circuit was assigned to accurately represent the relationships appearing in the electrochemical process under study.

Wear resistance tests were performed using the ball-on-disc method. Anton Paar's tribometer device was used for the tests. The conditions under which the tests were performed were the following: wear diameter of 3 mm, normal force $F_n = 5 \text{ N}$, linear velocity $v = 5 \text{ cm/s}$. The tests were performed at room temperature in an air atmosphere. The tests were performed at 20 000 cycles. One cycle was taken as one complete rotation of the specimen around its axis.

4. RESULTS AND DISCUSSION

The surface topography of the hybrid coatings at the microscale shows a topographical structure typical of coatings obtained by MSPVD (Fig. 1a). The coatings contain morphological defects in the form of small pores and microcracks. In addition, they contain scratches on the surface, which are residues from the process of mechanical preparation of the substrate for coating, grinding, and polishing. This indicates that the coatings are not thick enough to accurately reflect the substrate to be coated. Chemical composition analysis EDS showed the presence of reflections suitable for the coatings under study, i.e. Cr, Ti, O, and N. The morphology of the CrN/TiO₂ hybrid coatings at the nanoscale shows a dependence on the number of ALD cycles. CrN/TiO₂(200) and CrN/TiO₂(500) coatings show wavelike morphology similar to that of CrN coating. This shows that the thin ALD coating accurately reflects the morphology of the PVD coating. In the case of the CrN/TiO₂(1000) coating, nanostructured granularity was observed (Fig. 1b).

Observation of the brittle fracture structure of the tested coat-

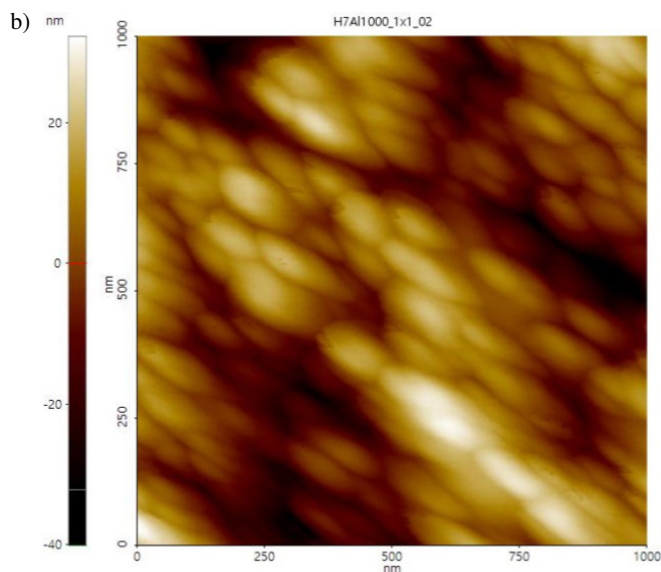
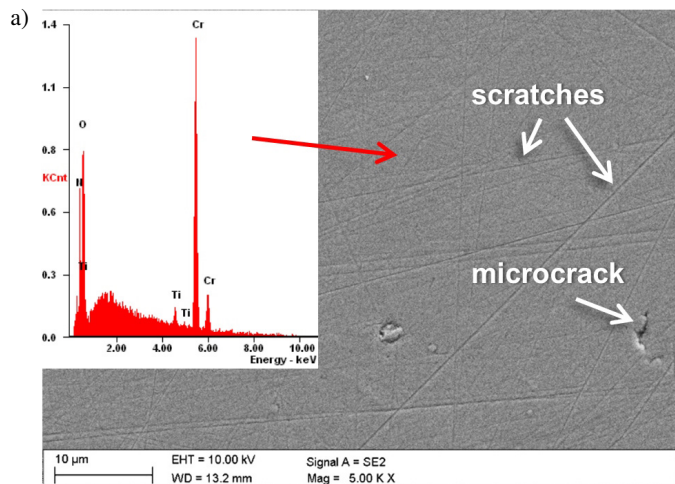


Fig. 1. a) Topography of CrN/TiO₂(500) coating, SEM with EDS analysis, b) Morphology of CrN/TiO₂(1000) coating, AFM

ings revealed that the coatings, as intended, contain two layers (Fig. 2). The layer near the substrate is chromium nitride, which shows a dense compact structure suitable for the T-zone according to the Thornton model [17]. The thickness of the CrN coating is $1.3 \pm 0.2 \mu\text{m}$. CrN coating is uniformly covered by a thin titanium oxide layer, the thickness of which depends on the number of ALD cycles and is $6 \pm 1 \text{ nm}$, $16 \pm 1 \text{ nm}$, and $32 \pm 1 \text{ nm}$ for 200, 500, and 1,000 cycles, respectively.

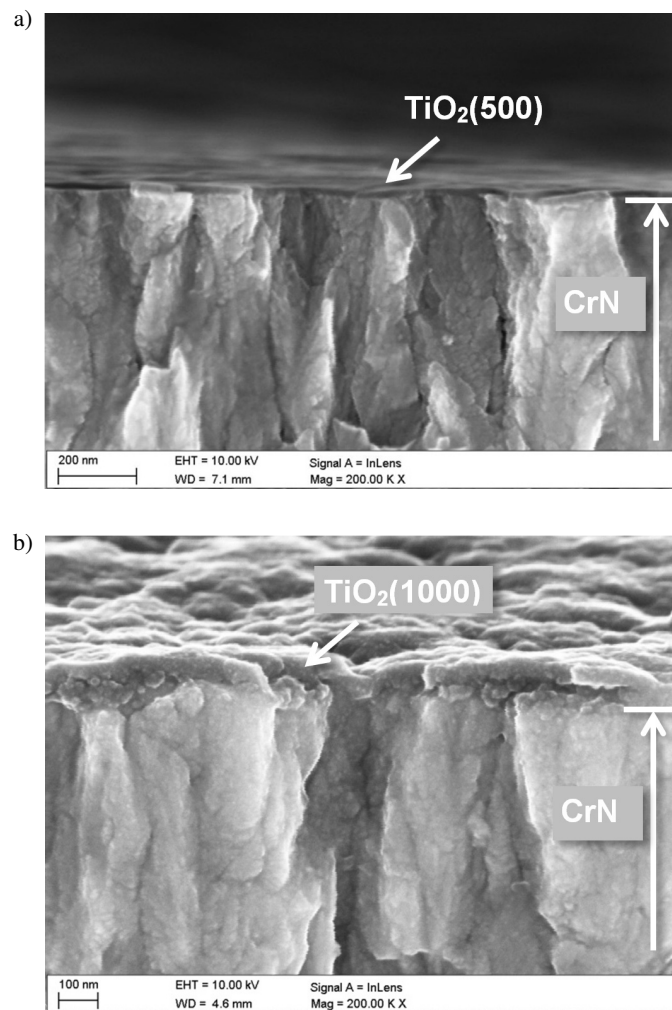


Fig. 2. Fracture of the hybrid coating: a) CrN/TiO₂(500), b) CrN/TiO₂(1000)

As a result of TEM research on the microstructure of lamellas made of CrN/TiO₂ hybrid coatings, it was found that the tested coatings had a multi-layered structure (Fig. 3a). The first layer from the substrate with thickness of about 100 nm is the so-called adhesive layer, consisting of pure chromium. The next layer is crystalline CrN chromium nitride with the cubic lattice Fm-3m (225), confirmed by diffraction analysis. The transition from the pure chromium layer to chromium nitride is relatively smooth, with no clearly delineated boundary between them. Both these layers form a PVD coating with thickness of about 1.4 μm. It has a titanium oxide layer obtained by the ALD method. This layer tightly adheres to the PVD coating, creating uniform coverage thickness in each tested fragment.

The tested areas of TiO₂ coating obtained in 500 ALD cycles show an amorphous structure (Fig. 3b). The study of the chemical composition of micro-areas confirms the presence of chemical elements appropriate for a given zone on the cross-section of the coating.

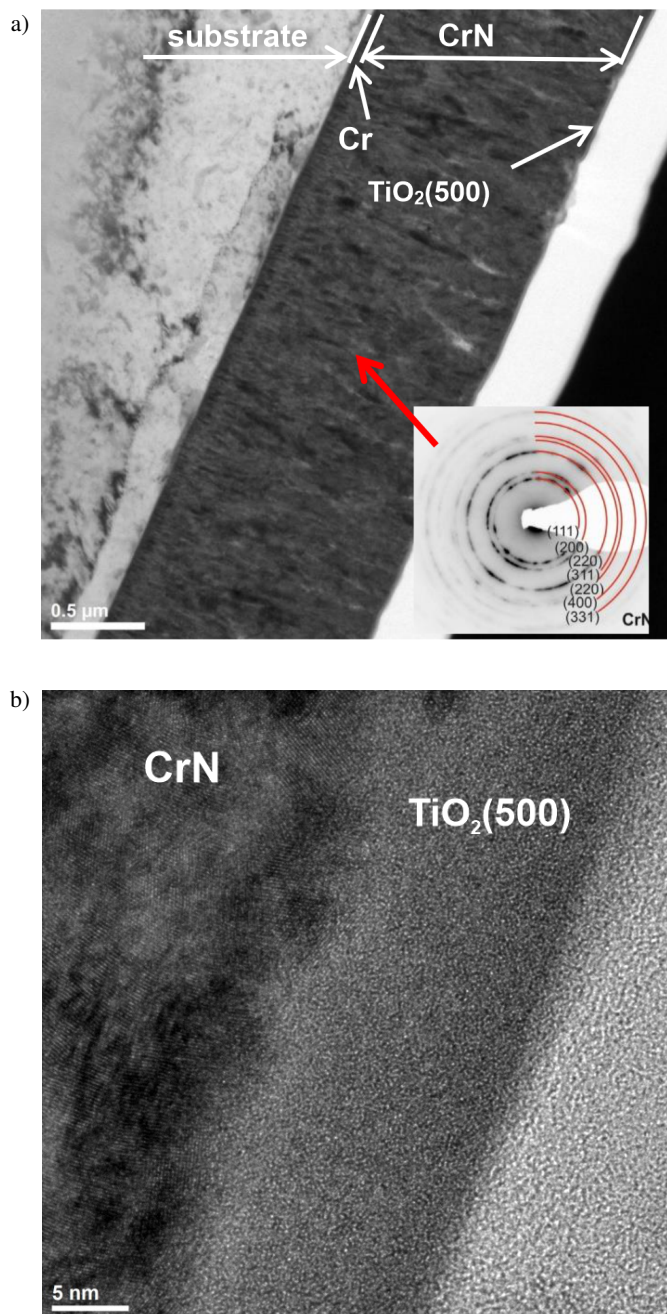


Fig. 3. Structure (TEM-BF) of CrN/TiO₂(500) hybrid coating: a) cross-sectional view of coating with diffraction pattern from CrN area, b) view of TiO₂ ALD layer

The study of hybrid coatings using Raman spectroscopy is shown in Fig. 4. The Raman spectrum from the CrN/TiO₂(1000) sample contains the characteristic bands of titanium oxide TiO₂ with a tetragonal structure from the space group I4₁/amd (141), i.e. anatase (144, 395, 517, 636 cm⁻¹).

No Raman bands were found on the obtained spectra in the remaining cases. This proves the lack of a crystalline structure of titanium oxide or no titanium oxide (in the case of the CrN coating, which was tested only as a reference sample).

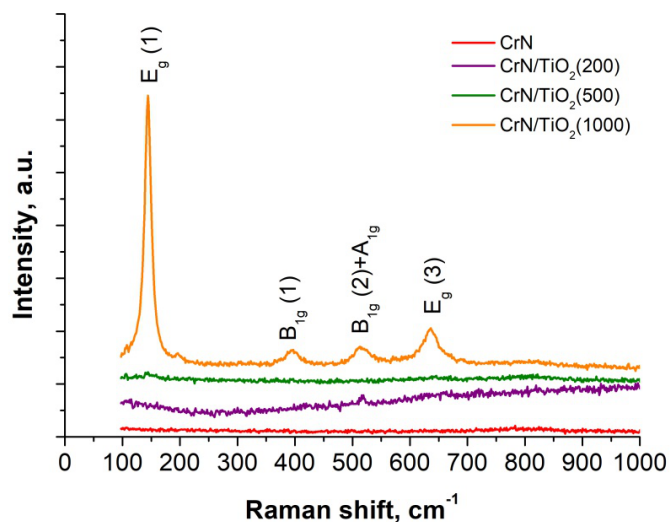


Fig. 4. Raman spectra of CrN and CrN/TiO₂ hybrid coatings deposited onto Al–Si–Cu alloy substrate

Based on the analysis of the contact angle of the uncoated Al–Si–Cu alloy surface and the samples coated with the tested coatings, it was found that the range of angle θ was within the range of $86^\circ \pm 3^\circ$ for the uncovered sample to $100^\circ \pm 2^\circ$. The contact angle values oscillate around the borderline value of the transition between the hydrophilic and hydrophobic states. However, it is worth noting that with the increasing number of ALD cycles in both ALD coatings and hybrid PVD / ALD coatings, the value of angle θ increases. At the same time, the coating of chromium nitride with a layer of titanium oxide in the PVD process causes the contact angle to change towards hydrophilicity (or rather to reduce hydrophobicity). The increase in hydrophobicity, in this case, may be associated with an increase in nano-roughness, which contributes to the formation of areas with air bubbles under the drops of water. This mechanism explains the so-called Cassie-Baxter condition [18]. Contact angle θ with diiodomethane ranges from $41^\circ \pm 2^\circ$ to $69^\circ \pm 1^\circ$. The values of the surface free energy are presented in Table 3. For all tested samples, there is a significant disproportion between the dispersion and polar components, i.e. $\gamma_d^s \gg \gamma_p^s$. The surfaces have an affinity for the non-polar SFE groups.

In the first stage of the DC tests, the steady-state potential (Table 4) was determined for the prepared samples by recording its value for 1 hour in a current-free system. The highest value was obtained for the Al–Si–Cu substrate material, while for all the samples with layers, whether obtained by PVD or ALD, as well as for the samples with hybrid coatings, the open-circuit potential value was lower by 80 to 100 mV. The second stage of the potentiodynamic study made it possible to determine, using the Tafel method (Table 4), the corrosion current density, polarization resistance, and corrosion potential, while in the case of the latter the differences in values were the same as the changes

Table 3

Contact angle measurements and surface energy calculated by the Owens–Wendt method

Coating	Wetting angle (°)		Surface free energy (mJ/m ²)		
	Distilled water	Diiodomethane	γ_p^s	γ_d^s	γ_s
Al–Si–Cu uncoated	86 ± 3	56 ± 2	4	27	31
TiO ₂ (200)	88 ± 1	54 ± 2	3.17	29.05	32.22
TiO ₂ (500)	94 ± 2	52 ± 3	0.84	34.07	34.91
TiO ₂ (1000)	97 ± 4	53 ± 3	0.35	34.56	34.92
CrN	100 ± 2	69 ± 1	1.22	27.7	23.92
CrN/TiO ₂ (200)	92 ± 3	41 ± 2	0.52	41.42	41.93
CrN/TiO ₂ (500)	93 ± 2	60 ± 1	2.43	26.55	28.9
CrN/TiO ₂ (1000)	96 ± 1	52 ± 3	0.51	34.57	35.07

Table 4

Potentiodynamic polarization parameters for samples in 3.5% NaCl solution

Sample	E_{ocp} , mV	E_b , mV	j_{corr} , $\mu\text{A}/\text{cm}^2$	E_{corr} , mV	R_{pol} , $k\Omega \cdot \text{cm}^2$	P_e , %*
Al–Si–Cu uncoated	–602	–542	0.72	–582	8.4	–
TiO ₂ (200)	–681	–644	1.50	–677	3.6	–133
TiO ₂ (500)	–676	–611	0.68	–670	13.3	37
TiO ₂ (1000)	–696	–607	0.77	–687	12.1	31
CrN	–691	–603	0.95	–685	10.6	21
CrN/TiO ₂ (200)	–708	–590	0.51	–705	19.1	56
CrN/TiO ₂ (500)	–707	–405	0.33	–724	67.9	88
CrN/TiO ₂ (1000)	–689	–484	4.1	–717	6.0	–40

* P_e – corrosion protection efficiency $\left(1 - \frac{R_{pol\text{substrate}}}{R_{pol\text{coating}}}\right) \times 100\%$

corresponding to the open-circuit potential. R_{pol} analysis made it possible to conclude that the majority of the applied coatings increased the material’s resistance to corrosion damage in the studied environment. The greatest increase in polarization resistance values was recorded for the hybrid coatings after 500 and 200 application cycles, while the CrN/TiO₂(1000) coating together with the TiO₂(200) coating had the lowest resistance to ions causing corrosion damage in the electrolyte tested, even lower than the uncoated material. Confirmation of the corrosion properties of the obtained coatings was obtained by comparing the values of the corrosion current density, which was recorded lowest for the hybrid-coated sample after 500 cycles, followed by the PVD+ALD-coated material after 200 application cycles. Higher j_{corr} values of the substrate material were registered for the CrN-coated sample, all ALD-only coated samples, and the worst performance was that of the CrN/TiO₂(1000) sample, whose corrosion current density was 6 times that of the uncoated sample.

Analyzing the anodic polarization curves, it was observed that the breakdown potential (E_b) value increased for the CrN/TiO₂(500) and CrN/TiO₂(1000) samples, indicating a wider range of protection of the material against brittleness due to exposure to Cl[–] ions (Table 4). The CrN/TiO₂(500) coated sample had the highest breakdown potential value, higher by an average of 200 mV than all PVD-coated and hybrid-coated materials after 200 cycles. Apart from this sample, only the CrN/TiO₂(1000) coated material still showed a higher potential value than the Al–Si–Cu uncoated sample.

To further analyze the electrochemical properties of the hybrid coated samples obtained, we performed tests using a second method, in an AC system, in a variable frequency range, and for the stationary potential of each material. Three impedance characteristics were determined from the recorded data: in the form of a Nyquist plot ($-Z_{imaginary} = f(Z_{real})$) (Fig. 5a) and a Bode plot (Fig. 5b) as the relationship $|Z| = f(\text{frequency})$ and $\Phi = f(\text{frequency})$.

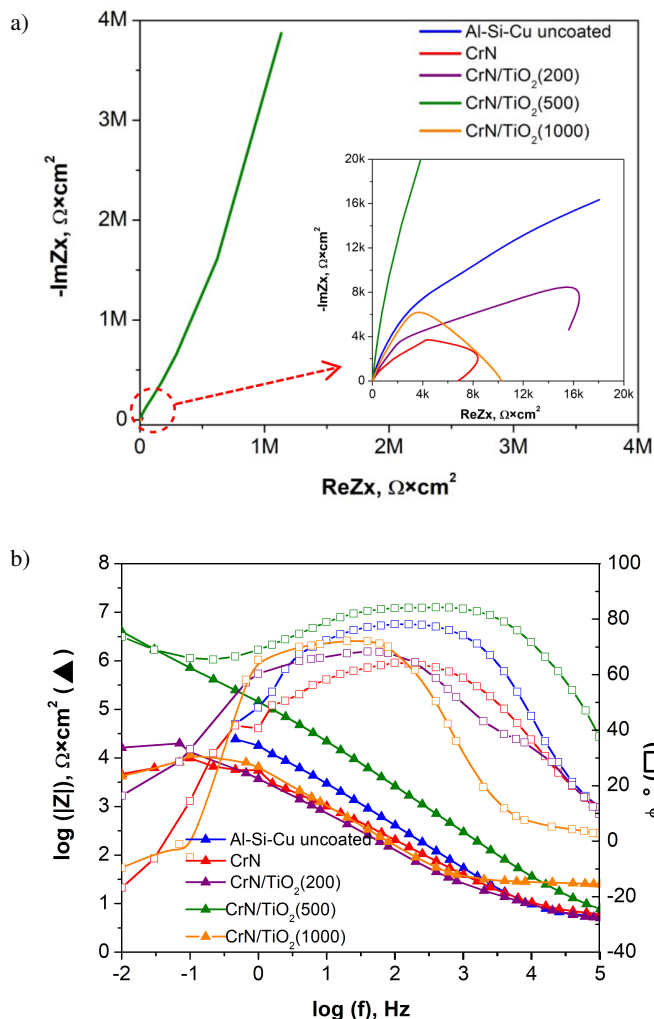


Fig. 5. Electrochemical impedance diagrams for uncoated Al–Si–Cu alloy and for one coated by CrN coating, and CrN/TiO₂ hybrid coatings: a) Nyquist representation, b) Bode representation

Complementary to the analysis of the impedance spectrum curves of the tested samples, an electrical equivalent circuit fitting was performed for which the impedance value was closest to the experimental data while ensuring the lowest possible number of elements to build such a circuit. Therefore, four types of equivalent circuits were used to best fit the calculation curve, depending on the type of sample (Fig. 6). In all surrogate circuits, the R1 element corresponds to the resistance of the electrolyte used for testing, and R2 represents the charge transfer resistance between the electrolyte and the phase boundary (uncoated and CrN sample), while R3 corresponds to the resistance in terms of coating and substrate (200 and 500 cycle hybrid sample) or the inductive resistance identified on the Nyquist diagram for the CrN/TiO₂(1000) sample. Q2 characterizes the properties of the double layer at the interface, Q3 is related to the capacitance between the layers and the material, and L2 corresponds to the inductor and the inductance value occurring in the low-frequency range (Table 5).

The value of the recorded resistance of the electrolyte varied in the range of 5 ÷ 25 Ω, the n-factor of the CPE element for the hybrid layers reached values above 0.88, and for the coat-

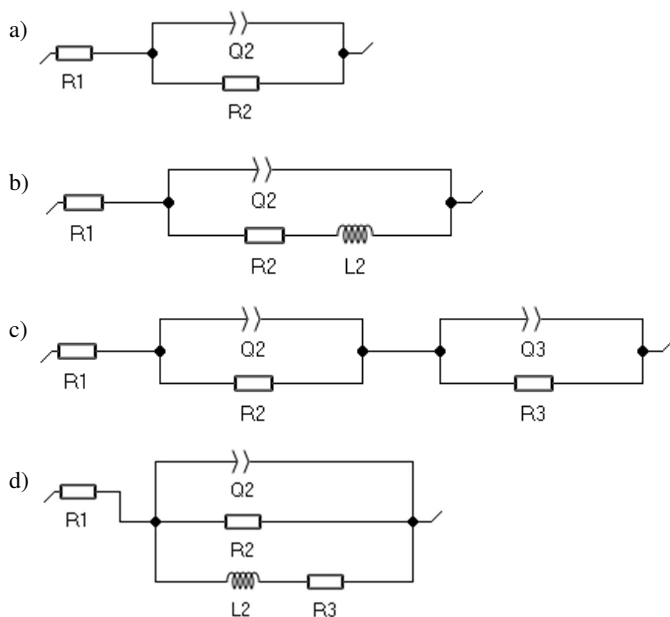


Fig. 6. Equivalent circuit that represents the impedance spectra for: a) uncoated substrate, b) CrN coating, c) CrN/TiO₂(200) and CrN/TiO₂(500), d) CrN/TiO₂(1000)

ings after 500 and 1000 application cycles they stood at 0.99 and 0.95, respectively, which shows the almost ideal capacitive character of this element.

The Nyquist plot of the impedance spectra (Fig. 5a) shows clear changes in the corrosion process rates for the different coatings applied. The highest impedance value, determined from real and imaginary components, was recorded for the sample with the hybrid coating after 500 application cycles, indicating its highest corrosion resistance in the tested environment. Smaller values of the slope coefficient of the spectra, compared to those of the substrate material sample, were present for all other coatings, whether after the PVD or PVD+ALD process. Furthermore, the Nyquist plot for the CrN coated sample and the CrN/TiO₂(1000) sample registered an inductive loop at low frequencies that may be related to the adsorption of aluminum ions, formed during the test, on the sample surface.

By analyzing the results shown in the Bode diagram (Fig. 5b), it can be confirmed that the best protection against corrosion damage, in the applied environment, was provided by applying the hybrid coating to the sample at 500 cycles. The highest impedance values were recorded for this material, across the entire range of frequencies investigated, while when comparing the spectra, the CrN/TiO₂(200) sample had the lowest values.

Based on the second representation of the Bode diagram, showing the frequency dependence of the phase shift angle, its highest value was found for the CrN/TiO₂(500) hybrid coating sample, for which it reached a value of more than 70° over almost the entire frequency range, from 1.6 Hz to 1000 Hz, with a maximum value of 84° recorded at average frequencies of 160–630 Hz. Among the other coatings, the high values of the phase shift angle were characterized by the hybrid coating sample after 1000 application cycles, which reached a maximum value of 71–72° at low-frequency values and in the narrower range from 6 to 60 Hz. The smallest angle ϕ was recorded for the CrN coated sample, whose maximum was recorded at 64° at 100–160 Hz.

The coefficient of friction determined during the ball-on-disc test of all tested samples ranges from 0.44 to 0.48 (Table 6). The estimated volume of material removed from the center of the wear path is 1.8 mm³. For a sample with a CrN coating, the volume is 0.8 mm³; for all tested hybrid coatings, it is 1.1 ÷ 1.2 mm³. This proves that both the PVD coating and the tested PVD/ALD hybrid coatings improve abrasion resistance

Table 5

Electrochemical impedance spectroscopy parameters

Coating	R1 [Ω]	Q2 [$\mu\text{F} \times \text{s}^{(\alpha-1)}$]	α_2	R2 [kΩ]	Q3 [$\mu\text{F} \times \text{s}^{(\alpha-1)}$]	α_3	R3 [kΩ]	L2 [kH]
Al-Si-Cu uncoated	5	13.15	0.79	58	–	–	–	–
CrN	6	50.75	0.62	7.9	–	–	–	3.9
CrN/TiO ₂ (200)	5	70.5	0.88	11	800.34	0.86	27	–
CrN/TiO ₂ (500)	6	4.22	0.99	$51.6 \cdot 10^3$	2.8	0.751	993	–
CrN/TiO ₂ (1000)	25	28.08	0.95	12	–	–	5.5	65

Table 6

Mean values of volume of the wear track of investigated samples

Coating	Tribology	
	Coefficient of friction μ	Volume of wear track, mm ³
Al–Si–Cu uncoated	0.46	1.8
CrN	0.45	0.8
CrN/TiO ₂ (200)	0.44	1.1
CrN/TiO ₂ (500)	0.47	1.1
CrN/TiO ₂ (1000)	0.48	1.2

of the coated material (Table 6). The volume of material removed in the case of hybrid coatings is about 30% greater than in the case of the CrN coating. This is undoubtedly related to the mechanism of nano-abrasive formation from the crumbling layer of titanium oxide on the surface of hybrid coatings in the initial phase of the test. Observations of the abrasion tracks confirmed that the tested coatings were worn and that the substrate was exposed (Fig. 7). The chemical composition analysis in the

micro-areas showed the presence of mainly aluminum and oxygen, which proves the formation of an aluminum oxide layer in the abrasion path. Moreover, the observation and EDS testing of the counter-sample made of cemented carbides showed the presence of aluminum and oxygen on its surface, which proves the formation of a build-up of the substrate material on its surface. The primary mechanism of damage caused by the test on the surface of the tested samples was abrasion.

5. SUMMARY

Hybrid technologies for producing surface layers show a significant advantage over traditional surface treatment methods because, thanks to the synergy mechanism, obtaining functional properties unattainable with each technology separately is possible. This work presents the results of tests of CrN/TiO₂ coatings obtained with the hybrid PVD/ALD method. The CrN coatings obtained by the PVD method and TiO₂ obtained by the ALD process, and the uncoated Al–Si–Cu substrate were also tested for comparative purposes. The titanium oxide coating was made in three variants, i.e. with a variable number of ALD cycles in the range of 200–500 at a constant temperature of 200°C. The main goal was to obtain high corrosion resistance while maintaining high abrasion resistance inherent in PVD coatings. Moreover, it was necessary to determine how the number of ALD cycles affects the PVD/ALD coatings produced on substrates made of Al–Si–Cu alloys.

The CrN/TiO₂(500) hybrid coating demonstrates the best electrochemical properties, for which the R_{pol} polarization resistance value is higher than the uncoated substrate by 88%, which is expressed by the P_e parameter (corrosion protection efficiency). It should also be noted that the CrN/TiO₂(200) coating also improves corrosion resistance, albeit to a lesser extent. On the other hand, the CrN/TiO₂(1000) coating showed worse R_{pol} and j_{corr} parameters than the uncoated substrate and most tested materials, proving its low anti-corrosion properties.

The electrochemical properties of the tested CrN/TiO₂ coatings are strictly dependent on the structure of the titanium oxide obtained by the ALD method on the surface of the PVD coating. As a result of structural studies of hybrid CrN/TiO₂ coatings, it was found that titanium oxide is amorphous or shows an anatase crystal structure depending on the number of ALD cycles. For a low number of cycles, i.e. 200, the titanium oxide on the surface of the chromium nitride is exclusively amorphous. For 500 ALD cycles, Raman spectroscopy already shows some TiO₂ anatase. However, TEM observations only show amorphous titanium oxide. This may indicate that for these conditions of titania synthesis by the ALD method, the formation of anatase nuclei in the amorphous matrix occurs, which is difficult to detect in TEM microscopic examinations. Titanium oxide in the CrN/TiO₂(1000) coating contains distinct crystallites of TiO₂ anatase, confirmed by Raman analysis. Distinct crystallites on the surface of this coating also showed in morphological studies, particularly AFM. Therefore, it should be assumed that with the increasing number of ALD cycles, i.e. the de facto thickness of the layer formed, nucleation of the TiO₂ anatase crystalline phase takes place from the amorphous phase

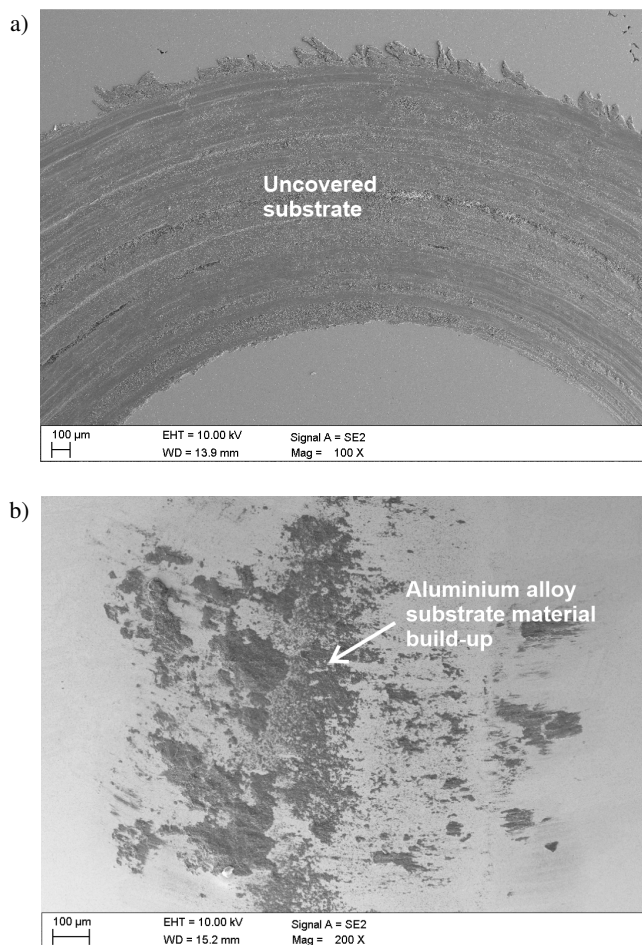


Fig. 7. a) Wear trace after the “ball-on-disc” wear test for CrN/TiO₂(500) coating, b) view of cemented carbides ball after the “ball-on-disc”

and then the growth of the resulting crystallites. The direction of changes from the amorphous phase through anatase and then rutile follows the Ostwald–Lussac law [19, 20].

As assumed, the tested PVD and PVD/ALD coatings show high tribological properties, improving the abrasion resistance of aluminum alloys as compared with the uncoated substrate. It should be noted, however, that due to the crumbling of the TiO₂ layer on the surface of hybrid coatings, they show slightly worse properties than the PVD coating.

6. CONCLUSIONS

Based on the research, the following conclusions were drawn:

- The corrosion resistance of the hybrid CrN/TiO₂(500) coating is distinctly higher than the corrosion resistance of other tested materials, in particular, the uncoated Al–Si–Cu substrate, and the one coated in single PVD and ALD technologies. High electrochemical properties result from the synergy of two combined surface treatment technologies, i.e. PVD and ALD.
- Hybrid CrN/TiO₂ coatings significantly improve the corrosion resistance of the coated Al–Si–Cu alloys when the titanium oxide obtained on the surface of chromium nitride is in an amorphous form.
- The amorphous/crystalline structure of the titanium oxide coating depends on the number of ALD cycles. The Ostwald–Lussac mechanism is responsible for forming the crystalline layer from the amorphous matrix.
- CrN and CrN/TiO₂ coatings provide a significant improvement in the abrasion resistance of the surface of the Al–Si–Cu coated aluminum alloy.

REFERENCES

- [1] D. Caliari, G. Timelli, B. Zabala, and A. Igartua, “Microstructural and tribological investigations of diecast and hard anodized AlSiCu alloys,” *Surf. Coat. Technol.*, vol. 352, pp. 462–473, 2018, doi: [10.1016/j.surfcoat.2018.07.084](https://doi.org/10.1016/j.surfcoat.2018.07.084).
- [2] P. Snopiński *et al.*, “Evolution of microstructure, texture and corrosion properties of additively manufactured AlSi10Mg alloy subjected to Equal Channel Angular Pressing (ECAP),” *Symmetry*, vol. 14, no. 4, p. 674, 2022, doi: [10.3390/sym14040674](https://doi.org/10.3390/sym14040674).
- [3] M. Uhrčík, P. Pačtek, M. Chalupová, P. Hanusová, and L. Kuchariková, “Analysis of the properties of EN AC 51200 aluminum alloy,” *Arch. Metall. Mater.*, vol. 65, no. 4, pp. 1437–1445, 2020, doi: [10.24425/amm.2020.133711](https://doi.org/10.24425/amm.2020.133711).
- [4] A.M. Titu, A.B. Pop, M. Năbialek, C.C. Dragomir, and A.V. Sandu, “Experimental modeling of the milling process of aluminum alloys used in the aerospace industry,” *Bull. Pol. Acad. Sci. Tech. Sci.*, vol. 69, no. 5, p. e138565, 2021, doi: [10.24425/bpasts.2021.138565](https://doi.org/10.24425/bpasts.2021.138565).
- [5] K. Labisz, “Laser surface treatment of cast Al–Si–Cu alloys,” *J. Achiev. Mater. Manuf. Eng.*, vol. 61, no. 2, pp. 63–86, 2013.
- [6] M. Staszuk *et al.*, “Investigations of TiO₂, Ti/TiO₂ and Ti/TiO₂/Ti/TiO₂ coatings produced by ALD and PVD methods on Mg–(Li)–Al–RE alloy substrates,” *Bull. Pol. Acad. Sci. Tech. Sci.*, vol. 69, no. 5, p. e137549, 2021, doi: [10.24425/bpasts.2021.137549](https://doi.org/10.24425/bpasts.2021.137549).
- [7] A. Mazurkiewicz, J. Smolik, J. Mizera, J. Kacprzyńska-Gołačka, M. Rydzewski, and M. Szota, “Composite layers “MgAl intermetallic Layer/PVD coating” obtained on the AZ91D magnesium alloy by different hybrid surface treatment methods,” *Arch. Metall. Mater.*, vol. 60, no. 2, pp. 1031–1035, 2015, doi: [10.1515/amm-2015-0255](https://doi.org/10.1515/amm-2015-0255).
- [8] K. Labisz, T. Tański, D. Janicki, W. Borek, K. Lukaszewicz, and L.A. Dobrzański, “Effect of laser feeding on heat treated aluminium alloy surface properties,” *Arch. Metall. Mater.*, vol. 61, no. 2, pp. 741–746, 2016, doi: [10.1515/amm-2016-0126](https://doi.org/10.1515/amm-2016-0126).
- [9] R. Bayón *et al.*, “Corrosion-wear behavior of PVD Cr/CrN multilayer coatings for gear applications,” *Tribol. Int.*, vol. 42, pp. 591–599, 2009, doi: [10.1016/j.triboint.2008.06.015](https://doi.org/10.1016/j.triboint.2008.06.015).
- [10] J.M. Lackner, W. Waldhauser, L. Major, J. Morgiel, M. Kot, and B. Major, “Nanocrystalline Cr/CrN and Ti/TiN multilayer coatings produced by pulsed laser deposition at room temperature,” *Bull. Pol. Acad. Sci. Tech. Sci.*, vol. 54, no. 2, pp. 175–180, 2006.
- [11] E.Y. Choi, M.Ch. Kang, D.H. Kwon, D.W. Shin, and K.H. Kim, “Comparative studies on microstructure and mechanical properties of CrN, Cr–C–N and Cr–Mo–N coatings,” *J. Mater. Process. Technol.*, vol. 187, pp. 566–570, 2007, doi: [10.1016/j.jmatproc.2006.11.090](https://doi.org/10.1016/j.jmatproc.2006.11.090).
- [12] M. Ürgen and A.F. Cakir, “The effect of heating on corrosion behavior of TiN- and CrN-coated steels,” *Surf. Coat. Technol.*, vol. 96, no. 2–3, pp. 236–244, 1997, doi: [10.1016/S0257-8972\(97\)00123-0](https://doi.org/10.1016/S0257-8972(97)00123-0).
- [13] C.X. Shan, X. Hou, K.-L. Choy, and P. Choquet, “Improvement in corrosion resistance of CrN coated stainless steel by conformal TiO₂ deposition,” *Surf. Coat. Technol.*, vol. 202, pp. 2147–2151, 2008, doi: [10.1016/j.surfcoat.2007.08.078](https://doi.org/10.1016/j.surfcoat.2007.08.078).
- [14] J. Leppäniemi, P. Sippola, M. Broas, J. Aromaa, H. Lipsanen, and J. Koskinen, “Corrosion protection of steel with multilayer coatings: Improving the sealing properties of physical vapor deposition CrN coatings with Al₂O₃/TiO₂ atomic layer deposition nanolaminates,” *Thin Solid Films*, vol. 627, pp. 59–68, 2017, doi: [10.1016/j.tsf.2017.02.050](https://doi.org/10.1016/j.tsf.2017.02.050).
- [15] Z. Wan *et al.*, “Enhanced Corrosion Resistance of PVD–CrN Coatings by ALD Sealing Layers,” *Nanoscale Res. Lett.*, vol. 12, p. 248, 2017, doi: [10.1186/s11671-017-2020-1](https://doi.org/10.1186/s11671-017-2020-1).
- [16] M. Staszuk *et al.*, “Investigations of TiO₂/NanoTiO₂ Bimodal Coatings Obtained by a Hybrid PVD/ALD Method on Al–Si–Cu Alloy Substrate,” *Coatings*, vol. 12, p. 338, 2022, doi: [10.3390/coatings12030338](https://doi.org/10.3390/coatings12030338).
- [17] J.A. Thornton, “The microstructure of sputter-deposited coatings,” *J. Vac. Sci. Technol. A*, vol. 4, p. 3059, 1986, doi: [10.1116/1.573628](https://doi.org/10.1116/1.573628).
- [18] P. Feng, Z. Dongdong, L. Xuanyong, and Z. Yu, “Recent progress in superhydrophobic coating on Mg alloys: A general review,” *J. Magnes. Alloy.*, vol. 9, no. 5, pp. 1471–1486, 2021, doi: [10.1016/j.jma.2020.08.024](https://doi.org/10.1016/j.jma.2020.08.024).
- [19] X. Yin and X. Wang, “Kinetics-driven crystal facets evolution at the tip of nanowires: A new implementation of the Ostwald–Lussac law,” *Nano Lett.*, vol. 16, no. 11, pp. 7078–7084, 2016, doi: [10.1021/acs.nanolett.6b03317](https://doi.org/10.1021/acs.nanolett.6b03317).
- [20] J. Shi, Z. Li, A. Kvit, S. Krylyuk, A.V. Davydov, and X. Wang, “Electron microscopy observation of TiO₂ nanocrystal evolution in high-temperature atomic layer deposition,” *Nano Lett.*, vol. 13, pp. 5727–5734, 2013, doi: [10.1021/nl403566u](https://doi.org/10.1021/nl403566u).